Open access • Journal Article • DOI:10.1063/1.1695594

Manipulation of two-dimensional arrays of Si nanocrystals embedded in thin SiO2 layers by low energy ion implantation — Source link

Caroline Bonafos, M. Carrada, Nikolay Cherkashin, H. Coffin ...+9 more authors

Published on: 06 May 2004 - Journal of Applied Physics (American Institute of Physics)

Topics: Ion implantation, Ion beam mixing, Gate oxide, Silicon and Nanocrystal

Manipulation of two-dimensional arrays of Si nanocrystals embedded in thin SiO 2 layers by low energy ion implantation

Caroline Bonafos, Marzia Carrada, Nikolay Cherkashin, H. Coffin, D. Chassaing, Gérard Benassayag, Alain Claverie, T. Müller, K.H. Heinig, M. Perego, et al.

Manipulation of two-dimensional arrays of Si nanocrystals embedded in thin SiO_2 layers by low energy ion implantation

C. Bonafos, M. Carrada, N. Cherkashin, H. Coffin, D. Chassaing, G. Ben Assayag, A. Claverie, T. Müller, K. H. Heinig, M. Perego, M. Fanciulli, P. Dimitrakis, and P. Normand

Citation: Journal of Applied Physics **95**, 5696 (2004); doi: 10.1063/1.1695594
View online: https://doi.org/10.1063/1.1695594
View Table of Contents: http://aip.scitation.org/toc/jap/95/10
Published by the American Institute of Physics

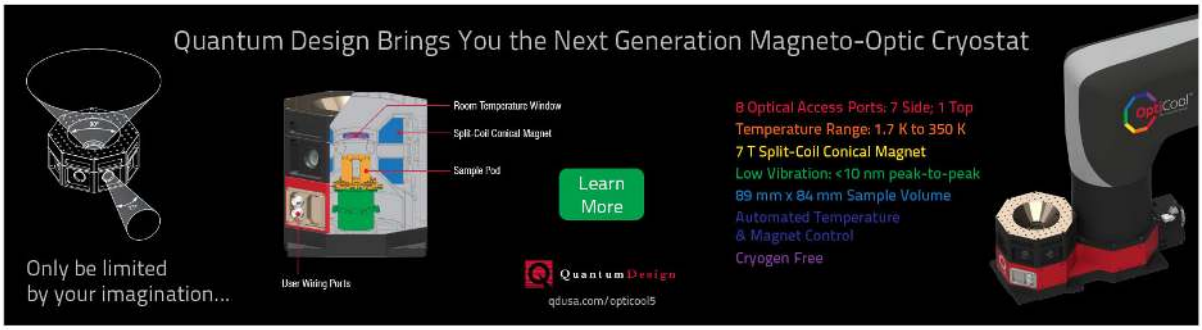

Manipulation of two-dimensional arrays of Si nanocrystals embedded in thin SiO_2 layers by low energy ion implantation

C. Bonafos,[a] M. Carrada, N. Cherkashin,[b] H. Coffin, D. Chassaing, G. Ben Assayag, and A. Claverie
nMat Group, CEMES-CNRS, 29 rue J. Marvig, 31055, Toulouse, France

T. Müller and K. H. Heinig
Forschungszentrum Rossendorf, Institut für Ionenstrahlphysik und Materialforschung, P.O. Box 510119, 01314 Dresden, Germany

M. Perego and M. Fanciulli
Laboratorio MDM—INFM, Agrate, Italy

P. Dimitrakis and P. Normand
Institute of Microelectronics, NCSR 'Demokritos', 15310 Aghia Praskevi, Greece

(Received 5 November 2003; accepted 12 February 2004)

In silicon nanocrystal based metal–oxide–semiconductor memory structures, tuning of the electron tunneling distance between the Si substrate and Si nanocrystals located in the gate oxide is a crucial requirement for the pinpointing of optimal device architectures. In this work it is demonstrated that this tuning of the "injection distance" can be achieved by varying the Si^+ ion energy or the oxide thickness during the fabrication of Si nanocrystals by ultralow-energy silicon implantation. Using an accurate cross-section transmission electron microscopy (XTEM) method, it is demonstrated that two-dimensional arrays of Si nanocrystals cannot be positioned closer than 5 nm to the channel by increasing the implantation energy. It is shown that injection distances down to much smaller values (2 nm) can be achieved only by decreasing the nominal thickness of the gate oxide. Depth profiles of excess silicon measured by time-of-flight secondary ion mass spectroscopy and Si nanocrystal locations determined by XTEM are compared with Monte-Carlo simulations of the implanted Si profiles taking into account dynamic target changes due to ion implantation, ion erosion, and ion beam mixing. This combination of experimental and theoretical studies gives a safe explanation regarding the unique technological route of obtaining Si nanocrystals at distances smaller than 5 nm from the channel: the formation of nanocrystals requires that the interface mixing due to collisional damage does not overlap with the range profile to the extent that there is no more a local maximum of Si excess buried in the SiO_2 layer.
[DOI: 10.1063/1.1695594]

I. INTRODUCTION

Memory devices consisting of a metal–oxide–semiconductor field-effect transistor (MOSFET) with nanocrystals (ncs) embedded within the gate oxide are promising candidates for high-storage-density low-power memory applications.[1,2] The use of a charge-storage floating gate made of mutually isolated ncs instead of a continuous poly-Si layer reduces charge losses through the underlying tunnel oxide by defect paths, thus allowing a scaling down of the tunnel oxide. For devices operation in the direct tunneling regime a fine control of the nanocrystal location is absolutely required since a change of less than 1 nm in tunnel oxide thickness dramatically affects programming properties (write/erase times and voltages) and data retention.[3,4]

Multidot floating gates consisting of Si or Ge ncs have been fabricated by different deposition techniques,[1,5] like thermal oxidation of $Si_{1-x}Ge_x$[6] or ion implantation followed by annealing.[7] The fabrication of nanocrystal memory devices by ultralow energy Si implantation and subsequent thermal treatment has been recently demonstrated.[8,9] This fabrication route is very attractive because of its ability to control the size and location of the narrow nanocrystal band and its compatibility with standard complementary MOS technology. In practice, high dose (typically $10^{16}\,cm^{-2}$) Si implantation in the 1 keV range into very thin (up to 10 nm thick) oxide layers followed by annealing (900–1000 °C) allows for the formation of two-dimensional arrays of Si ncs positioned at direct tunneling distances from the SiO_2/Si interface.[8] In principle, it is possible to accurately control the position of the nanocrystal band by changing the implantation[10] and annealing conditions, but up to now no systematic studies have been performed.

In this work, we show how the "injection distance" separating the nanocrystal layer edge and the SiO_2/Si interface (channel) can be tuned by varying either the ion implantation energy or the initial thickness of the SiO_2 layer. For this purpose, measurements of the injection distance as a function of these two parameters have been performed

[a]Electronic mail: bonafos@cemes.fr
[b]On leave from Ioffe Physico-Technical Institute, St. Petersburg.

TABLE I. Experimental conditions for three different sets of samples. Sets 1 and 2 are dedicated to the study of the effect of the implantation energy (for fixed dose, set 1 and for fixed Si excess for set 2) within a 10-nm-thick SiO_2 layer. Set 3 is used to examine the influence of a variation of the nominal oxide thickness for constant implantation conditions.

Set of sample	Nominal oxide thickness (nm)	Energy (keV)	Dose (cm^{-2})	Annealing conditions
	10	0.65	10^{16}	950 °C 30 min under N_2
	10	1	10^{16}	950 °C 30 min under N_2
1	10	2	10^{16}	950 °C 30 min under N_2
	10	3	10^{16}	950 °C 30 min under N_2
	10	5	10^{16}	950 °C 30 min under N_2
	10	1	10^{16}	950 °C 30 min under N_2
2	10	3	2.1×10^{16}	950 °C 30 min under N_2
	10	5	3.2×10^{16}	950 °C 30 min under N_2
	10	1	10^{16}	950 °C 30 min under N_2
3	7	1	10^{16}	950 °C 30 min under N_2
	5	1	10^{16}	950 °C 30 min under N_2

through conventional transmission electron microscopy (TEM) examination under out-of-Bragg and strongly underfocused bright field (Fresnel contrast imaging) conditions with a resolution better than 1 nm.[10,11] It is pointed out that with increasing implantation energy injection distances below 5 nm cannot be achieved, while injection distances as thin as 2 nm can be obtained by decreasing the initial oxide thickness from 10 nm down to 5 nm and using 1 keV Si ion energy. TEM results are discussed and correlated with time-of-flight secondary ion mass spectroscopy (TOF–SIMS) measurements of the Si excess depth profiles as well as with Dynamical TRIM (TRIDYN) simulations[12] taking into account surface sputtering, changes in stoichiometry as well as collisional mixing effects.

II. EXPERIMENTAL AND SIMULATION DETAILS

Three sets of samples have been examined. All sample details are summarized in Table I. The first one (set 1, Table I) consists of 10-nm-thick SiO_2 layers on (001) Si implanted with 10^{16} Si^+ ions/cm^2 at energies between 0.65 and 5 keV. The second set (set 2, Table I) consists of 10-nm-thick SiO_2 layers implanted at the same energies than set 1, but the Si^+ doses were chosen in such a manner that the peak concentration of the implanted Si reaches always 35 at. % (in SiO_2). These doses, predicted by TRIDYN,[12] are $10^{16}\,cm^{-2}$, $2.1\times10^{16}\,cm^{-2}$, and $3.2\times10^{16}\,cm^{-2}$ at energies of 1, 3, and 5 keV, respectively. For the third set of samples (set 3, Table I), the implantation energy and dose are fixed at 1 keV and 10^{16} Si^+ cm^{-2}, respectively, but the initial oxide thickness is varied from 10 nm down to 5 nm. It should be noted that these implantations (except 0.65 keV into 10-nm-thick SiO_2 layer) result in the amorphization of a thin layer of the Si substrate below the SiO_2. The thickness of this amorphous layer varies from a few nanometers to more than 20 nm at the highest ion energy. After implantation, the samples were annealed in a conventional furnace under N_2 atmosphere at 950 °C for 30 min. Finally, a 60-nm-thick poly-Si layer was deposited on top of the oxide to help in visualizing the SiO_2 surface in TEM images.

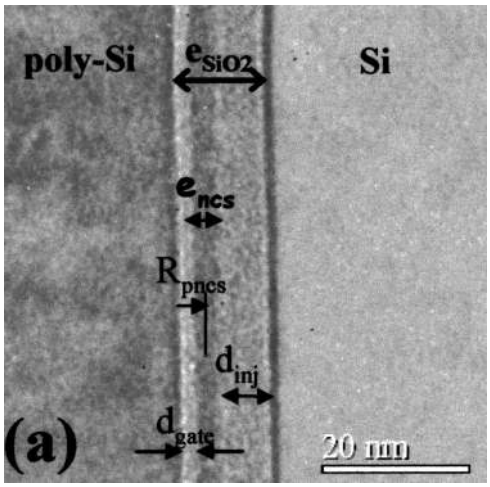

FIG. 1. XTEM image taken under strongly underfocused bright field conditions ($\Delta f = -400$ nm). The sample is a 10-nm-thick SiO_2 film on (001) Si implanted at 10^{16} Si^+ cm^{-2} and 1 keV energy, which was subsequently furnace annealed at 950 °C for 30 min under N_2 ambient. The nanocrystal layer appears as a thick black line surrounded by two white fringes.

Specimens from all samples were prepared for cross-sectional TEM (XTEM) observations using the standard procedure involving mechanical polishing and ion milling. Images were taken on a CM30 Philips TEM equipped with a standard LaB_6 electron source operating at 300 keV and having a nominal resolution of 0.19 nm. For measuring the location of the nanocrystal layer in the SiO_2 layer, we have used a previously developed method for the fast and accurate measurement of characteristics distances in such systems.[11] By using Fresnel contrast, i.e., by illuminating the sample with a highly coherent electron beam and imaging it in strongly underfocused out-of-Bragg bright-field conditions, a pair of (black/white or white/black) Fresnel fringes appears on each interface separating the SiO_2 from the nanocrystal layer and from the electrodes. Figure 1 shows such an image ($\Delta f = -400$ nm) and reveals the structure of an initially 10-nm-thick SiO_2 layer implanted at 1 keV with a dose of 10^{16} Si^+ cm^{-2}, which was subsequently annealed. The layer of Si excess, which appears as a thick black line surrounded by two white fringes, is extremely well depth-localized and forms a quasi "two-dimensional (2D) array" of ncs. Microdensitometric analysis of such images is performed using an on-line charge coupled device camera and image processing. On the obtained densitometric profiles, all distances of interest can be precisely measured (±0.5 nm) by locating the inflexion points of each pair of black and white fringes originating from the different interfaces. On all the samples, we have measured the different characteristic distances as indicated in Fig. 1, i.e., the SiO_2 thickness (e_{SiO_2}), the injection distance (d_{inj}), the width of the nanocrystal layer (e_{ncs}), the distance between the "center of mass" of the nanocrystal array and the gate (R_{pncs}), and the gate distance (d_{gate}). For the sample shown in Fig. 1, this nanocrystal layer is 2.5 ± 0.5 nm thick, located at an "injection distance" (d_{inj}) of 7.8 ± 0.5 nm from the SiO_2/Si interface and at a gate distance (d_{gate}) of 2 ± 0.5 nm from the poly-Si capping layer. High resolution electron microscopy (HREM) observations have also been

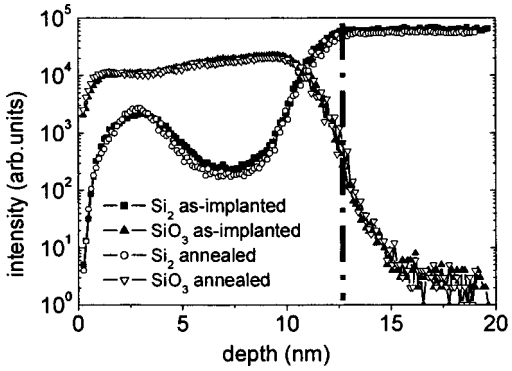

FIG. 2. TOF–SIMS depth profiles of a 10-nm-thick SiO_2 layer on (001) Si implanted at 1 keV and with a dose of 10^{16} Si^+ cm^{-2} as-implanted (closed squares) and after furnace annealing at 950 °C for 30 min under N_2 ambient (open circles). Only $_{28}Si_{n=2}$ signals are shown here even if $_{28}Si_{n>2}$ signals are also detected. The vertical dash-line indicates the SiO_2/Si interface as measured on the TEM images of Fig. 1.

performed for calibrating the magnification used for distance measurements on one hand and on the other hand for imaging the quality of the SiO_2/Si interface.

TOF–SIMS has been used to measure the depth distribution of Si excess in Si^+ implanted oxides[13,14] by using an ION-TOF CAMECA IV dual beam TOF–SIMS. Sputtering for depth profiling was accomplished by Cs^+ ions at 0.5 keV and 7.3 nA, rastering over a 150×150 μm^2 area. The analysis was performed in negative polarity by using Ga^+ ions operating at 25 keV and 2.8 pA, rastering over 50×50 μm^2 area. TOF–SIMS data were normalized using the ^{30}Si signal of bulk Si in order to remove variations of the signal's intensity due to fluctuations of the Ga current. A linear time-to-depth conversion was performed assuming a constant sputter rate and using a reference oxide of known thickness to measure the sputter velocity. The set of TOF–SIMS profiles presented in Fig. 2 shows the effect of annealing on the distribution of excess Si in such thin layers. Before annealing, the implanted Si excess obeys a classical Gaussian peak shape centered at about 3 nm, which has sharpened after annealing due to the nucleation of ncs in the Si excess layer detected by TEM. Moreover, the slope at the interface becomes steeper and, consequently, a more pronounced denuded zone has formed between the Si excess layer and the interface. It should be noted that no significant Si excess redistribution was found after annealing. This is due to the very low diffusivity of Si in SiO_2.[15,16]

The binary collision code TRYDIN[12] was used to predict the target stoichiometry after high-dose low-energy Si^+ implantation into SiO_2. It extends the commonly used TRIM program[17] to high-fluence implantation conditions and includes dynamic target changes, i.e., changes due to ion implantation, ion sputtering, and ion beam mixing. The displacement energies E_d for both Si and O were assumed to be 8 eV. This value proved to yield satisfactory agreement between earlier TRIDYN simulations of ion mixing and experiments.[18]

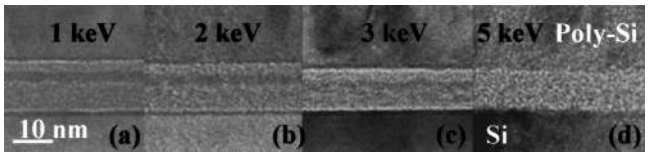

FIG. 3. Series of XTEM images (from set 1, Table I) taken under defocused bright-field conditions. Si^+ was implanted at energies increasing from 1 to 5 keV into 10-nm-thick SiO_2 layers on top of (001) Si with a constant dose of 10^{16} Si^+ cm^{-2}. The samples were subsequently furnace annealed at 950 °C for 30 min under N_2 ambient.

III. RESULTS AND DISCUSSION

A. Effect of the implantation energy

For tuning the nanocrystal position within the SiO_2 layer, our first attempt was to vary the implantation energy according to samples set 1 of Table I. Figure 3 shows the corresponding XTEM images showing the effect of increasing the implantation energy in 10-nm-thick SiO_2 layers. As ion energy increases, the nanocrystal layer shifts deeper in the SiO_2 layer, i.e., closer to the Si/SiO_2 interface. The HREM micrograph of Fig. 4 shows isolated ncs with a mean size of 2–3 nm in that region. Surprisingly, no ncs are observed in HREM for 5 keV implantation.

The scheme of Fig. 5 depicts the evolution of all the characteristic distances as a function of the implantation energy. The observed behavior differs for ion energies above and below 2 keV. Indeed, when increasing the implantation energy from 0.65 to 1.5 keV, the distance between the ''center of mass'' of the nanocrystal array and the gate (R_{pncs}) increases from 3 to 4 nm and the width of the nanocrystal layer slightly increases from 2 to 3 nm. Consequently, the injection distance decreases only from 8 to 7 nm. The depth position of the ncs agrees with the peak location of the Si implantation profiles predicted by TRIDYN[19] (from 2.3 to 4.1 nm when the energy varies from 0.65 to 1.5 keV and for 10^{16} Si/cm^{-2}). The larger width of the nanocrystal layer reflects the profile broadening with increasing energy. An overall swelling of the SiO_2 layers by 2 nm is observed, which is found to be independent of the ion energy ($e_{SiO_2} = 12$ nm).

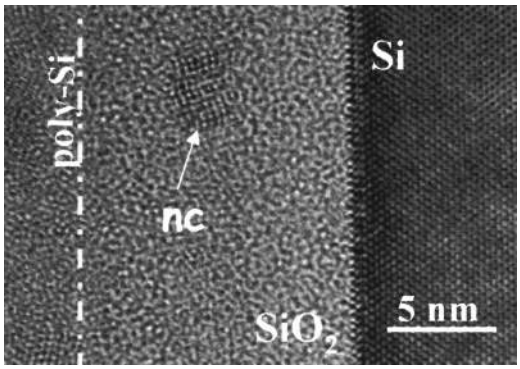

FIG. 4. Cross-sectional HREM image showing lattice fringes of an isolated Si nanocrystal in the SiO_2 layer. The sample (from set 1, Table I) is the one shown on Fig. 1, i.e., a 10-nm-thick SiO_2 film on (001) Si implanted with 10^{16} Si^+ cm^{-2} at 1 keV energy, which has subsequently been annealed at 950 °C for 30 min in N_2 ambient.

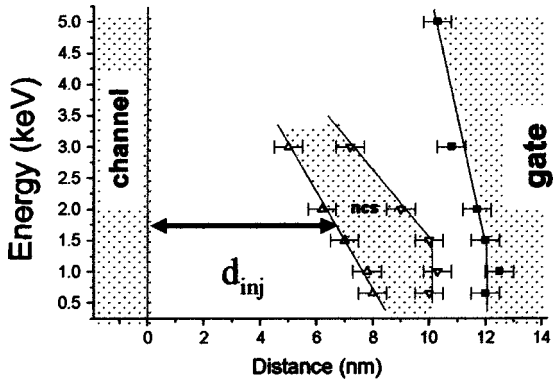

FIG. 5. Cross-sectional scheme depicting the evolution of the characteristic distances for the variation of the implantation energy from 0.65 to 5 keV (y axis) of samples from set 1, Table I. These distances (SiO_2 thickness, injection distance, width of the ncs layer), defined in Fig. 1, were measured on the TEM images of Fig. 3 and are plotted on the x axis. Up triangles: distance between the bottom edge of the nanocrystal layer and the Si substrate (injection distance). Down triangles: distance between the top edge of the nanocrystal layer and the Si substrate. Squares: distance between the polysilicon layer and the Si substrate (SiO_2 thickness). All the distances are measured with an accuracy of ± 0.5 nm.

Increasing the ion energy from 2 to 3 keV, the distance between the center of mass of the nanocrystal array and the gate grows further and, consequently, the injection distance decreases to 5 nm. The swelling of SiO_2 is reduced to 1 nm, while the width of the nanocrystal layer decreases to 2.2 nm. It is worth noting that after 5 keV implantation, while no ncs are detected, the thickness of the SiO_2 layer is the same than before implantation (swelling equals to zero). For this sample HREM imaging of the SiO_2/Si deep interface reveals some unusual undulations and an atomic roughness of a few atomic planes over periods of about 10 nm (see Fig. 6).

In order to compensate the decrease of the Si peak concentration with increasing ion energy, the experiment was repeated with ion doses adjusted to obtain a constant peak concentration of 35 at. % Si excess. By doing so, a similar process of nanocrystal formation is expected for all ion energies.

Figure 7 shows for samples set 2 of Table I that indeed the nanocrystal layer shifts closer to the SiO_2/Si interface at ion energies increasing from 1 to 3 keV. However, the swelling of the SiO_2 layer decreases with increasing energy although the ion dose has been doubled. HREM imaging [Fig. 7(d)] shows that already after 3 keV implantation the SiO_2/Si interface exhibits a roughness, which has previously been observed at lower dose for 5 keV implants only. After implantation at 5 keV no ncs are detected by TEM within the SiO_2 layer. In contrast, the SiO_2/Si interface is very rough and becomes faceted [see Fig. 7(c)]. Stacking faults and multiple twins on {111} planes are found in the substrate close to the interface. Small disoriented grains are also found on top of the interface and result from twinning [see Fig. 7(e)]. Due to this poor interface quality, it is clear that Si implantation in very thin SiO_2 layers with such high ion energies and doses is not appropriate for memory fabrication.

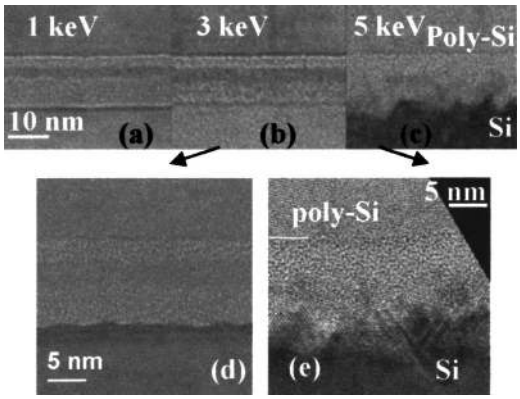

FIG. 7. Series of XTEM images [(a)–(c)] of samples from set 2, Table I taken under defocused bright-field conditions. (d) is the HREM image of the rough SiO_2/Si interface for the 3 keV implantation. For the highest energy (5 keV) the HREM image (e) shows a rough and faceted SiO_2/Si interface as well as stacking faults and twins in the Si substrate close to the SiO_2/Si interface.

Depth profiles of Si excess in SiO_2 have been measured by TOF–SIMS on samples set 2 after annealing. Figure 8 shows the evolution of these different profiles as the ion energy increases from 1 to 5 keV. The concentration of excess Si in SiO_2 is related to the yield of Si dimers. For 1 keV, a characteristic Gaussian profile of Si excess centered at 3 nm has been found, which is well separated from the Si/SiO_2 interface. For 3 keV, the profile has shifted deeper into the SiO_2 and is broader as expected when increasing the ion energy. Also, the interface has broadened to an error-function-like shape indicating ion beam mixing of the

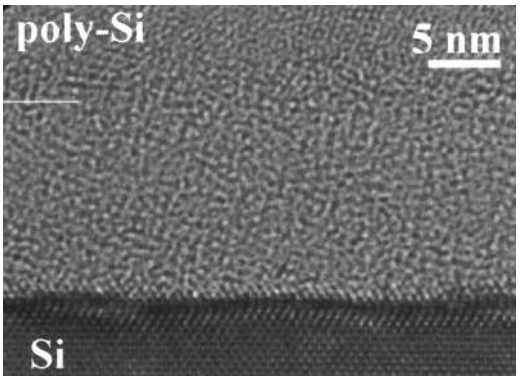

FIG. 6. HREM cross-sectional image of the sample implanted with 5 keV Si ions to a dose of 10^{16} cm^{-2} showing the rough SiO_2/Si interface.

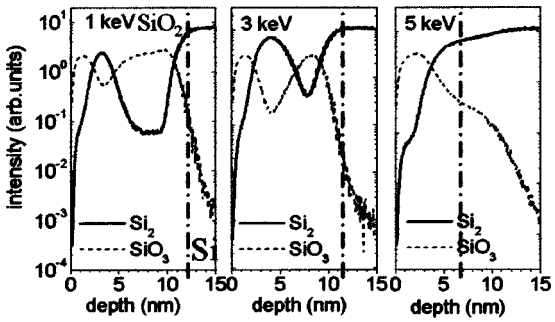

FIG. 8. TOF–SIMS depth profiles for samples of set 2, Table I. Only the SiO_3 and $_{28}Si_{n=2}$ signals are shown despite other $_{28}Si_{n>2}$ signals were also detected. The dashed vertical lines indicate the SiO_2/Si interfaces as measured on the TEM images of Fig. 7.

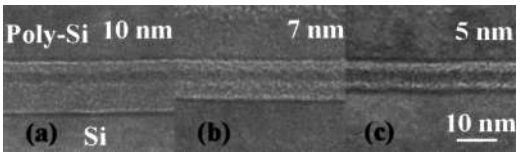

FIG. 9. Series of XTEM images of sample set 3, Table I, taken under defocused bright-field conditions.

Si/SiO_2 interface. The Si enriched regions due to implantation and interface mixing get closer to each other at increasing ion energy. Both regions of Si excess start to overlap at 3 keV and have merged for 5 keV. The Gaussian contribution of the Si^+ implantation is then hardly detectable, while the error-like function has broadened and even shifted from the interface towards the surface. No local maximum of Si excess is maintained in the SiO_2 layer. In contrast, this SiO_2 layer is thinner than expected and this is an indication that some transfer of implanted Si atoms towards the interface took place.

Thus, whatever doses and energies used to implant Si in 10-nm-thick SiO_2 layers, the 2D arrays of Si ncs cannot be positioned closer than 5 nm to the substrate, i.e., the injection distance is 5 nm at least. At high dose and energy, the implanted silicon is partially or totally absorbed by the deep SiO_2/Si interface.

B. Effect of the initial oxide thickness

Another option to decrease the injection distance is to keep fixed implantation conditions and to decrease the nominal oxide thickness. We have studied by TEM (see Fig. 9) the evolution of the characteristic distances for samples set 3 of Table I. The measurements are summarized in the scheme of Fig. 10. When the oxide thickness decreases, both, the depth position of the ncs and the width of the nanocrystal layer remain constant. A constant swelling of about 2 nm of the SiO_2 layer is observed. Consequently, when decreasing the nominal oxide thickness from 10 to 5 nm, the injection distance decreases from 7.2 to 2 nm, respectively. For the structure shown in Fig. 9(c), the nanocrystal layer is 2.5 nm wide, located at 2 nm from the channel and 2.5 nm from the gate.

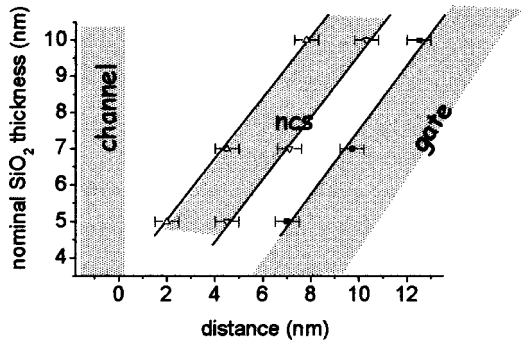

FIG. 10. Cross-sectional scheme depicting the evolution of the characteristic distances for the variation of the oxide thickness from 5 to 10 nm (y axis) of samples from set 3, Table I. These distances (SiO_2 thickness, injection distance, width of the ncs layer), defined in Fig. 1, were measured on the TEM images of Fig. 9 and are plotted on the x axis. Up triangles: distance between the bottom edge of the nanocrystal layer and the Si substrate (injection distance). Down triangles: distance between the top edge of the nanocrystal layer and the Si substrate. Squares: distance between the polysilicon layer and the Si substrate (SiO_2 thickness). All the distances are measured with an accuracy of ± 0.5 nm.

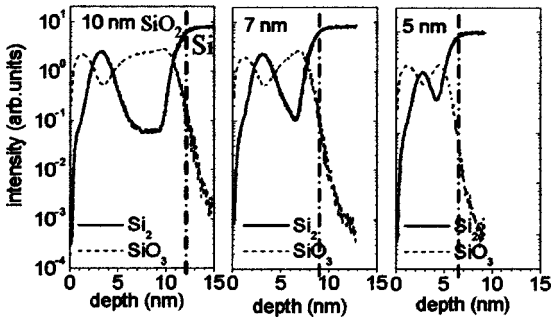

FIG. 11. TOF–SIMS depth profiles for the samples of set 3, Table I. Only the SiO_3 and $^{28}Si_{n=2}$ signals are shown despite other $^{28}Si_{n>2}$ signals were also detected. The dashed vertical lines indicate the SiO_2/Si interfaces as measured on the TEM images of Fig. 9.

TOF–SIMS profiles of these samples are shown in Fig. 11. When reducing the oxide thickness from 10 down to 7 nm, the two regions of Si excess, i.e., the Gaussian-like implantation profile and error-function-like ion beam mixed interface, get closer to each other. After implantation into 5-nm-thick SiO_2 layer, the implant profile peaks at a slightly lower concentration value but its general shape remains unaffected. The width of the ion beam mixed interface increases only marginally when reducing the oxide thickness and, consequently, the Si excess peak obtained by implantation remains unaltered. In all cases, the Si implantation profiles exhibit a local maximum within the SiO_2 layers, which corresponds to the nanocrystal layer detected by TEM.

When implanting Si at low energy (1 keV) and reducing the nominal oxide thickness down to 5 nm, a nanocrystal layer can always be formed within a SiO_2 layer at a depth corresponding to the maximum of the implanted profile. This layer can be positioned at a tuneable distance from the SiO_2/Si interface which can be rendered as small as 2 nm.

C. Discussion

From the results obtained by TEM and TOF–SIMS, one may conclude that a 2D layer of Si ncs well-separated from the Si/SiO_2 interface can be found only if the corresponding Si excess profile exhibits a local maximum in the SiO_2. This maximum is preserved as far as the ion beam induced interface broadening does not overlap with (dominate) the implantation profile. In order to understand the origin of the redistribution of Si and O atoms at the interface, TRIDYN simulations[12] were performed to calculate the Si depth profiles for implantations into thin SiO_2 layers of various thicknesses on top of a Si substrate. Results from these simulations are plotted in Fig. 12 for 1 keV implantations in 5-, 7-, and 10-nm-thick SiO_2 layers. 1 keV Si implantation into a 10-nm-thick SiO_2 layer results in a Gaussian profile of Si excess, which is well separated from the sharp Si/SiO_2 interface. There exists a denuded zone of about 3 nm between the Si-rich SiO_2 region and the interface. When reducing the oxide thickness down to 7 nm, the range profile and the

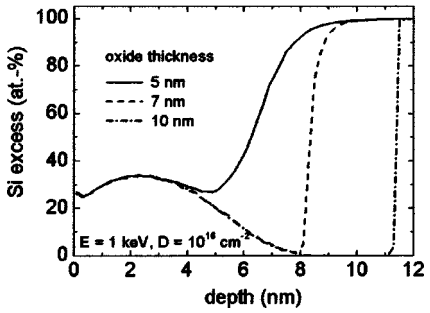

FIG. 12. Si excess depth profiles predicted by TRIDYN for the implantation conditions of set 3 of Table I.

interface get closer to each other, but still do not merge. The situation becomes critical when implanting a 5-nm-thick SiO_2 layer as the two components of the overall concentration profile start to overlap and sum up. This behavior is not only due to reduction of the distance between the projected range and the interface, but also due to an interface broadening by ion beam mixing. Indeed, as the damage energy (energy received by the target atoms through nuclear collisions with the incident Si atoms and the O and Si recoils) becomes non-negligible in the interfacial region, some oxygen atoms are displaced from the SiO_2 layer into the Si substrate while Si atoms are backscattered from the Si substrate into the SiO_2 layer. Such backscattering is very efficient in the experimental situations described in this article since most of the collision events involve very small energy transfers and thus very large scattering angles. For this reason, the signal from the interface evolves towards an error function-like profile when increasing interfacial mixing. However, this broadening is not sufficient to smear out the local maximum due to the Si implantation itself even after implantation into a 5-nm-thick SiO_2 layer. It is striking that these TRIDYN predictions perfectly describe the SIMS profiles and thus provide a solid basis for the understanding of the observed phenomena.

TRIDYN was also used to predict the effect of varying the Si ion beam energy from 0.65 to 5 keV at an ion dose of 10^{16} Si/cm^{-2} for a 10-nm-thick SiO_2 layer. Results are shown in Fig. 13. Again, the overall Si excess depth distribution is the sum of two contributions, one from the implant, the other one from the mixed interface. By increasing the energy from 0.65 up to 2 keV, the implant profile (Gaussian shape) shifts towards greater depths and broadens. For these

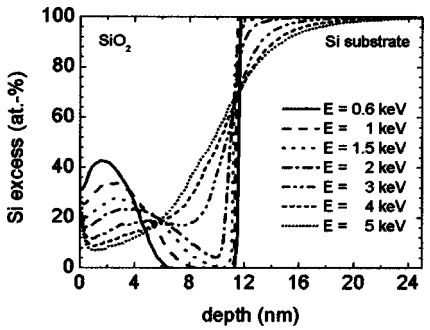

FIG. 13. Si excess depth profiles predicted by TRIDYN for the implantation conditions of set 1 of Table I.

low energy ion implantations, the damage energy (recoil cascade) is confined to the SiO_2 layer and ion beam mixing of the interface remains negligible. The joint Si excess profile (implantation+mixing) still exhibits a local maximum in the SiO_2 layer. Nanocrystals are observed by TEM at this peak maximum after annealing. When increasing the energy further, ion beam mixing displaces Si atoms from the substrate into the SiO_2 by backward scattering and an error-like profile of Si excess is observed. Ion beam mixing of the SiO_2/Si interface sets in at approximately 2 keV when the SiO_2 layer is 10 nm thick. Above 3 keV, the ion beam mixing becomes so strong that its contribution to the Si enrichment of the oxide layer becomes larger than the contribution from the implant species itself. Finally, after a 5 keV implant, the Si concentration continuously increases with increasing depth. Again, it is striking to note that these simulations very well reproduce the experimental SIMS results of Fig. 8 including the transition regime between 3 and 5 keV.

Thus, the stoichiometry of low-energy Si^+ implanted thin SiO_2 films on Si can be predicted nicely by TRIDYN, i.e., by considering only collisional phenomena. This striking result can be explained by the extremely small diffusivity of Si in SiO_2,[15,16] which renders the redistribution of Si during annealing almost undetectable by SIMS. Nevertheless, the diffusional mass transport is sufficient to allow the formation of ncs in the Si excess region. As a rule of thumb, a criterion for the formation of two-dimensional arrays of ncs insulated from the SiO_2/Si interface is that a local maximum remains present into the SiO_2 layer after implantation.

To understand the mechanisms which take place in the layers during annealing, it is very important to keep in mind that for all the implantations studied in this work (except 0.65 keV in 10-nm-thick SiO_2) the Si substrate has been amorphized from the Si/SiO_2 interface to a depth which increases with energy and dose and typically ranges from 3 to 20 nm. Thus during annealing, two mechanisms are always in competition, the solid phase epitaxial (SPE) regrowth of the amorphous region of the Si substrate and the phase separation of the Si excess from the SiO_2, i.e., the nucleation of ncs in the SiO_2. If the interface is sharp (negligible mixing) and the implant profile is well defined, the two phenomena do not interact: the amorphous Si layer recrystallizes up to its initial position within milliseconds at 950 °C leaving an atomically flat interface. Nanocrystals are formed independently as a band centered at the peak on the Si excess profile. The presence of a planar interface on the deep side and of a band of ncs in front drives the slow diffusing Si atoms left in between towards one of these trapping sites during annealing, preferably towards the planar interface where the concentration of Si atoms is minimum (equilibrium concentration Ci*). These concentration gradients help denuding the injection oxide during annealing. In such cases, the swelling of the layer only depends on the implanted dose. This is observed in all samples implanted at 1 keV whatever the initial oxide thickness that we have investigated and up to 2 keV in 10-nm-thick SiO_2 layers.

In contrast, after a high dose 3 keV implant, ncs still form at the peak maximum but the swelling of the SiO_2 layer is smaller (1 nm instead of 2 nm) than after a 1 keV implant

with half of that dose. TEM images show undulations of the (100) interface. These are clear indications that part of the implanted Si has been transferred to the substrate where it grows in epitaxy leading to the formation of Si islands on this interface. This is a confirmation that the interface does behave as a trap for free Si atoms.

After 5 keV implants, the Si profile continuously decreases from the interface towards the surface before and after annealing and consequently isolated ncs are not formed. The very broad interface region cannot sharpen itself during our standard annealing into a flat interface. The observation of stacking faults and microtwins in the substrate suggests that the SPE regrowth took selectively place on a very rough, (111) faceted, interface. One can infer that during annealing, the Si rich SiO_2 region close to the interface performs phase separation through the progressive transfer of Si atoms towards the interface. This transfer results in the nonhomogeneous epitaxial growth of the interface which becomes rougher as the growth proceeds.

IV. CONCLUSION

The influence of the ion energy and of the nominal SiO_2 thickness on the depth position of Si ncs obtained by low-energy ion beam synthesis has been explored. When increasing the implantation energy from 0.65 keV down to 3 keV for a fixed ion dose or for a fixed Si excess obtained by implantation into 10-nm-thick SiO_2, the injection distance can be reduced at least to 5 nm. For an ion energy above 3 keV, no ncs are found by TEM within the SiO_2 layer.

On the contrary, the injection distance can be decreased down to 2 nm by decreasing the oxide thickness from 10 nm down to 5 nm for a given implantation energy of 1 keV. This would then allow a nanocrystal charging by direct electron tunneling from the Si substrate (channel). In all cases, the observation of Si ncs by TEM always coincides with the presence of a local maximum of the Si excess profile within the SiO_2 layer as detected by TOF–SIMS and predicted by TRIDYN simulations.

Our results show further that the fabrication a 2D array of ncs sufficiently insulated from the Si/SiO_2 interface is the result of a trade-off between two parameters, the variation of the ion beam energy and the SiO_2 layer thickness. Indeed, the formation of ncs requires that the interface mixing due to collisional damage does not overlap with the range profile to the extend that there is no more a local maximum of Si excess buried in the SiO_2 layer. The contrary can be observed for strong interface mixing and/or a too small separation between the implantation profile and the Si/SiO_2 interface. No ncs have been found by TEM under such conditions.

For these reasons, ultralow-energy implantation (<1 keV) appears have a decisive advantage over more classical implantation. Moreover, TRIDYN has been proven to be extremely efficient in reproducing all the experimental results herein reported and gives hope for the development of a predictive simulation tool for the engineering of memory devices making use of ncs as charge storage elements.

ACKNOWLEDGMENTS

This work was partially supported by the European Commission through the Growth Project No. G5RD/2000/00320-NEON (nanoparticles for electronics). The authors want to thank D. Tsoukalas of IMEL, Demokritos Center, of Athens without whom this work would not have been carried out.

[1] S. Tiwari, F. Rana, H. I. Hanafi, A. Hartstein, E. F. Crabbé, and K. Chan, Appl. Phys. Lett. **68**, 1377 (1996).
[2] H. I. Hanafi, S. Tiwari, and I. Khan, IEEE Trans. Electron Devices **ED43**, 1553 (1996).
[3] S. Tiwari, F. Rana, K. Chan, L. Shi, and H. Hanafi, Appl. Phys. Lett. **69**, 1232 (1996).
[4] P. Normand *et al.*, Appl. Phys. Lett. **83**, 168 (2003).
[5] G. Ammendola *et al.*, J. Vac. Sci. Technol. B **20**, 2075 (2002).
[6] Y. C. King, T. J. King, and C. Hu, IEEE Trans. Electron Devices **ED48**, 696 (2001).
[7] P. Normand, D. Tsoukalas, E. Kapetanakis, J. van den Berg, D. G. Armour, J. Stoemenos, and C. Vieu, Electrochem. Solid-State Lett. **88**, 1 (1998).
[8] P. Normand *et al.*, Nucl. Instrum. Methods Phys. Res. B **178**, 74 (2001).
[9] P. Dimitrakis *et al.*, Mater. Sci. Eng., B **101**, 14 (2003).
[10] M. Carrada *et al.*, Mater. Sci. Eng., B **101**, 204 (2003).
[11] G. Ben Assayag, C. Bonafos, M. Carrada, P. Normand, D. Tsoukalas, and A. Claverie, Appl. Phys. Lett. **82**, 200 (2003).
[12] W. Möller and W. Eckstein, Nucl. Instrum. Methods Phys. Res. B **2**, 814 (1984).
[13] M. Perego, S. Ferrari, S. Spiga, E. Bonera, M. Fanciulli, and V. Soncini, Appl. Phys. Lett. **82**, 121 (2003).
[14] M. Perego, S. Ferrari, M. Fanciulli, G. Ben Assayag, C. Bonafos, M. Carrada, and A. Claverie, J. Appl. Phys. **95**, 257 (2004).
[15] D. Tsoukalas, C. Tsamis, and P. Normand, J. Appl. Phys. **89**, 7809 (2001).
[16] D. Mathiot, J. P. Schunck, M. Perego, M. Fanciulli, P. Normand, C. Tsamis, and D. Tsoukalas, J. Appl. Phys. **94**, 2136 (2003).
[17] J. P. Biersack and L. G. Haggmark, Nucl. Instrum. Methods **174**, 257 (1980); http://www.srim.org
[18] W. Möller, Nucl. Instrum. Methods Phys. Res. B **15**, 688 (1986).
[19] T. Müller, K. H. Heinig, and W. Möller, Appl. Phys. Lett. **81**, 3049 (2002).